Explicit IMF By-dependence of energetic protons and the ring current

Lauri Holappa[1] and Natalia Buzulukova[2]

[1]University of Oulu
[2]UMCP/NASA GSFC

November 24, 2022

Abstract

The most important parameter driving the solar wind-magnetosphere interaction is the southward (Bz) component of the interplanetary magnetic field (IMF). While the dawn-dusk (By) component of the IMF is also known to play an important role, its effects are usually assumed to be independent of its sign. Here we demonstrate for the first time a seasonally varying, explicit IMF By-dependence of the ring current and Dst index. Using satellite observations and a global magnetohydrodynamic (MHD) model coupled with a ring current model, we show that for a fixed level of solar wind driving the flux of energetic magnetospheric protons and the growth-rate of the ring current are greater for By<0 (By>0) than for By>0 (By<0) in Northern Hemisphere summer (winter). While the physical mechanism of this explicit By-effect is not yet fully understood, our results suggest that IMF By modulates magnetospheric convection and plasma transport in the inner magnetosphere.

Posted on 24 Nov 2022 — CC-BY-NC 4 — https://doi.org/10.1002/essoar.10510279.1 — This a preprint and has not been peer reviewed. Data may be preliminary.

Explicit IMF B_y-dependence of energetic protons and the ring current

L. Holappa[1,2,3], **N.Y. Buzulukova**[2,3]

[1]Space Physics and Astronomy Research Unit, University of Oulu, Finland
[2]University of Maryland, College Park, MD, USA
[3]NASA Goddard Space Flight Center, Greenbelt, MD, USA

Key Points:

- We show for the first time that there is an explicit By-dependence in the ring current/proton precipitation and in the inner magnetosphere.
- During NH summer (winter) the ring current fluxes/proton precipitation and the rate of change of the Dst index are stronger for $B_y < 0$ ($B_y > 0$).
- The B_y-dependence of the ring current and energetic proton fluxes is reproduced by a global coupled MHD-ring current model.

Corresponding author: Lauri Holappa, lauri.holappa@oulu.fi

Abstract

The most important parameter driving the solar wind-magnetosphere interaction is the southward (B_z) component of the interplanetary magnetic field (IMF). While the dawn-dusk (B_y) component of the IMF is also known to play an important role, its effects are usually assumed to be independent of its sign. Here we demonstrate for the first time a seasonally varying, explicit IMF B_y-dependence of the ring current and Dst index. Using satellite observations and a global magnetohydrodynamic (MHD) model coupled with a ring current model, we show that for a fixed level of solar wind driving the flux of energetic magnetospheric protons and the growth-rate of the ring current are greater for $B_y < 0$ ($B_y > 0$) than for $B_y > 0$ ($B_y < 0$) in Northern Hemisphere summer (winter). While the physical mechanism of this explicit B_y-effect is not yet fully understood, our results suggest that IMF B_y modulates magnetospheric convection and plasma transport in the inner magnetosphere.

1 Introduction

The interaction between solar wind, interplanetary magnetic field (IMF) and the Earth's magnetic field is dominated by the north-south (B_z) component of IMF, which is the most important driver of dayside reconnection [*Dungey*, 1961], and thus the energy input into the magnetosphere. The dawn-dusk (B_y) component of IMF is also known play an important role, leading, e.g., to a B_y-dependence of the ionospheric convection patterns [*Heppner and Maynard*, 1987; *Cowley et al.*, 1991; *Ruohoniemi and Greenwald*, 2005; *Thomas and Shepherd*, 2018]. It is also known that IMF B_y modulates the dayside reconnection rate by affecting, e.g., the geometry of the merging line [*Sonnerup*, 1974; *Laitinen et al.*, 2007; *Trattner et al.*, 2012], its effect on the magnetospheric response is usually assumed to be symmetric with respect to its sign. However, several studies [*Friis-Christensen et al.*, 1972, 2017; *Smith et al.*, 2017; *Holappa and Mursula*, 2018; *Workayehu et al.*, 2021; *Holappa et al.*, 2021] have shown that there is a strong IMF B_y-dependence in auroral currents which is not symmetric with the B_y sign. This so-called explicit B_y-dependence is especially strong in the AL index (measuring the westward electrojet), which is about 40% stronger for $B_y > 0$ than for $B_y < 0$ in Northern Hemisphere (NH) winter, or under negative tilt angle of the Earth's magnetic dipole with respect to the Sun-Earth line. In Northern Hemisphere summer (or during positive dipole tilt) the B_y-dependence is reversed.

The B_y-dependence of the auroral electrojets is at least partly due to a B_y-dependence of electron precipitation and ionospheric conductance. *Holappa et al.* [2020] showed that the fluxes of energetic (> 30 keV) precipitating electrons in the dawn sector (measured by the National Oceanic and Atmospheric Administration (NOAA) Polar Operational Environmental satellites, POES) are modulated by IMF B_y similarly as the westward electrojet (greater precipitation for $B_y < 0$ in NH summer and $B_y > 0$ in NH winter). The B_y-dependence of electron precipitation implies a similar B_y-dependence of ionospheric conductance. Recent studies [*Holappa et al.*, 2021; *Weimer and Edwards*, 2021] have indeed found a similar IMF B_y-dependence of ionospheric conductance, maximizing in the dawn sector.

The physical mechanism of the explicit B_y-effect is still not fully understood. As the above recent studies indicate, understanding how IMF B_y modulates the magnetospheric energetic particles and their precipitation into ionosphere are of key importance. An important question is whether the ring current also exhibits an explicit B_y-dependence. Possible explicit IMF B_y effects in the inner magnetoshere have not been analyzed, although it has been suggested that IMF B_y plays a role in skewing of the inner magnetosphere electric field as observed in Energetic Neutral Atom (ENA) emissions [*C:son Brandt et al.*, 2002].

A viable method for studying the coupling between IMF B_y and the ring current is to use physics-based numerical models, such as global magnetohydrodynamic (MHD) models coupled with the ring current models of the inner magnetosphere [*de Zeeuw et al.*, 2004; *Tóth et al.*, 2005; *Zhang et al.*, 2007; *Buzulukova et al.*, 2010a; *Glocer et al.*, 2013]. While the MHD physics is not sufficient for describing energetic particle populations, the global MHD models can be coupled with kinetic inner magnetosphere models, such as the Comprehensive Inner Magnetosphere-Ionosphere (CIMI) model [*Fok et al.*, 2014, 2021], designed for modeling the ring current and radiation belt physics.

The goal of this paper is to quantify the B_y-dependence of magnetospheric electrons and protons and the ring current using global modeling with a coupled model and satellite measurements. We will use the Space Weather Modeling Framework (SWMF) [*Tóth et al.*, 2005] coupled with the CIMI model. With this capability we are able to model also the B_y-dependence of the ring current fluxes. We will compare the modeling results to measurements of NOAA POES measurements of energetic magnetospheric protons and the *Dst* index.

This paper is organized as follows. In Section 2 we will introduce the data and the models in our analysis. The results from the global coupled model and satellite measurements are given in Sections 3 and 4, respectively. Finally we discuss our results and give our conclusions in Section 5.

2 Data and methods

2.1 Global 3D MHD BATS-R-US model coupled with CIMI

We use the global 3D BATS-R-US MHD code [*Tóth et al.*, 2005] coupled with the Comprehensive Inner Magnetosphere and Ionosphere (CIMI) model [*Fok et al.*, 2014] and Ridley ionospheric electrodynamics (RIM) module [*Ridley et al.*, 2004]. BATS-R-US and RIM are parts of Space Weather Modeling Framework (SWMF) developed at University of Michigan. The CIMI coupled code is developed at NASA GSFC Geospace Physics laboratory. For this study we use an ideal one-fluid anisotropic version of BATS-R-US MHD with grid resolution 1/8 R_E in the near-Earth region. The total number of grid points is $\sim 8{\times}10^6$. It is acknowledged that magnetic field reconnection in ideal MHD model is defined by numerical resistivity, however multiple studies of substorms with different MHD codes [*Fedder et al.*, 1995; *Raeder et al.*, 2010; *Birn and Hesse*, 2013; *Gordeev et al.*, 2017; *Merkin et al.*, 2019; *Keesee et al.*, 2021] confirm that this approach works reasonably well for the Earth's magnetosphere (although with some caveats). Global MHD model provides a reasonable solution for 3D structure of currents, magnetic field and plasma parameters (bulk velocity, pressure and density). In the inner magnetosphere, additional physics should be included to describe the ring current effects. This is done by dynamic two-way coupling of MHD solution and the ring current solution in order to describe energy-dependent gradient drifts of the ring current population with energies ∼1 - 200 keV. Details of the coupling methodology can be found in [*de Zeeuw et al.*, 2004; *Glocer et al.*, 2013].

Solution for ionospheric electric field potential is provided by RIM with ionospheric conductivity calculated from an empirical relation between field-aligned currents and ionospheric conductivity specified with the Assimilative Mapping of Ionospheric Electrodynamics (AMIE) model [*Ridley et al.*, 2004].

In this paper we present the results of two runs with positive/negative IMF GSM B_y = +5/-5 nT for the dipole tilt 20° in XZ GSM plane, corresponding to summer in northern hemisphere (NH). The value of tilt is kept fixed through the two runs. Except IMF B_y all run parameters are kept the same. Two runs are made with static IMF input solar wind V_x = - 500 km/sec; $V_y = V_z = 0$; IMF $B_x = 0$; solar wind density n=3 cm^3; solar wind temperature T = 200000 K. The first 2h of simulations are done with B_z = 3 nT, and the next 6h of simulations are done with static B_z = -5 nT.

2.2 NOAA POES data and Dst index data

In this paper we use energetic particle measurements from NOAA15-NOAA19 satellites in 1995-2019. The measurements from different NOAA satellites have been calibrated for instrument degradation and other issues [*Asikainen and Mursula*, 2011, 2013]. The POES satellites measure protons with two orthogonal (0° and 90°) detectors, measuring both precipitating and trapped particles. To compare the POES measurements to the modeled omnidirectional proton fluxes we average the 0° and 90° fluxes of the lowest energy channel (30-80 keV).

To quantify the intensity of the ring current we use the *Dst* index. Instead of the standard (Kyoto) *Dst* index (which is currently only available until 2014 in the final form) we use the University of Oulu version (called the *Dxt* index, available at `dcx.oulu.fi`), which also corrects some minor errors in the standard *Dst* index [*Karinen and Mursula*, 2005; *Mursula et al.*, 2008]. However, we note that practically identical results can be obtained using the standard *Dst* index.

3 Results: IMF B_y effect in CIMI fluxes and energy content

Figure 1a and 1b show the omnidirectional fluxes of 56 keV protons for the last timestep (8.00 h) of the two runs at the geomagnetic equatorial plane (minimum B field plane) for $B_y = +5$ nT and $B_y = -5$ nT, respectively, calculated from CIMI output. For two runs with different By the proton flux is stronger in premidnight and dusk sectors. This reflects the well-known dawn-dusk asymmetry of the ring current during the storm main phase [*Hamilton et al.*, 1988; *Liemohn et al.*, 2001; *Buzulukova et al.*, 2010b; *Yakovchouk et al.*, 2012].

In addition to well-known dawn-dusk ring current asymmetry, proton fluxes in Figure 1 exhibit a strong B_y-dependence. The proton fluxes are greater for negative B_y than for positive B_y. This B_y-dependence is strongest in the dusk and premidnight sectors where the fluxes are also largest overall. Figure S1 in the supporting material is similar to Figure 1 shows that the omnidirectional (56 keV) electron flux in the dawn sector exhibits a similar B_y-dependence as protons in the dusk sector, showing larger value of fluxes for the run with negative B_y, in agreement with earlier based on NOAA POES measurements of > 30 keV electrons [*Holappa et al.*, 2020].

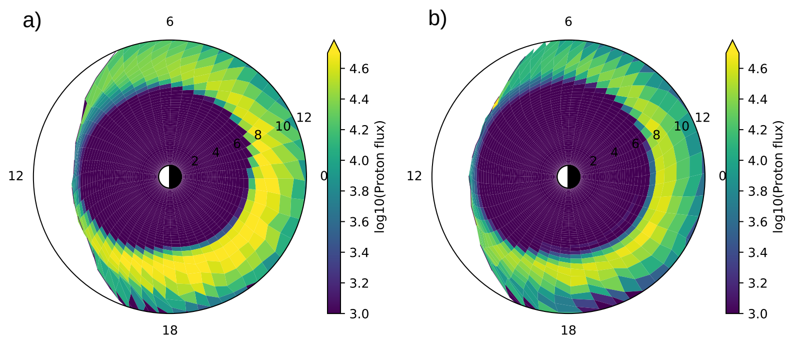

Figure 1. Equatorial omnidirectional fluxes of 56 keV protons for a) the run with $B_y < 0$ b) $B_y > 0$. Flux units are $1/cm^2/sr/s/keV$ in log-10 scale. The fluxes are shown for the last timesteps (8.00 h) of the two runs. Sun is from the left. Labels indicate magnetic local time and radial distance (in Earth radii).

Figure 2a shows the total energy content of the ring current calculated from the proton CIMI model for the two runs with opposite polarities of IMF B_y after the IMF B_z is turned southward at $t = 2$ h. While the evolution of ring current energy is very similar for both signs of IMF B_y during $t = 3..6$ h, negative B_y yields clearly greater ring current energy during the last two hours of the runs. The same B_y-dependence is seen in Figure 2b, which shows the pressure-corrected Dst indices (Dst^*) [*O'Brien and McPherron*, 2000] calculated from the ring current energies (U) in Figure 2a by the Dessler-Parker-Sckopke (DPS) relationship ($Dst^* = 3.98 \cdot 10^{-30} \cdot U$ [keV]) [*Dessler and Parker*, 1959].

Both Figures 1 and 2 demonstrate that the ring current fluxes, energy content and the modeled Dst index show explicit IMF B_y-dependence with stronger ring current and larger fluxes for negative B_y in northern hemisphere summer.

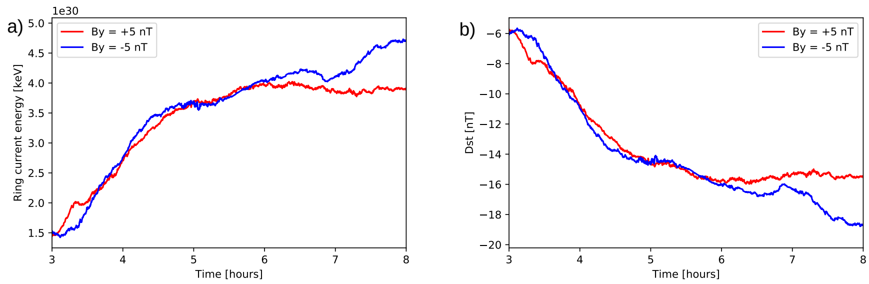

Figure 2. a) Simulated total energy of the ring current protons as a function of the simulation time for the signs of IMF B_y. b) Dst^* indices calculated from the total proton energy using the Dessler-Parker-Sckopke relationship.

4 Results: IMF B_y-effect in measured energetic protons and the Dst index

To support and extend results presented in the previous section, we study the B_y-dependence of energetic (30-80 keV) protons, measured by NOAA POES satellites. For quantifying the B_y-dependence of the particle fluxes we use similar methodology as *Holappa et al.* [2020], by sorting the measured particle fluxes by IMF B_y and the the *Newell et al.* [2007] coupling function, designed to represent the dayside reconnection rate at the magnetopause (MP)

$$\frac{d\Phi_{MP}}{dt} = v^{4/3} B_T^{2/3} \sin(\theta/2)^{8/3}, \tag{1}$$

where $B_T = \sqrt{B_z^2 + B_y^2}$ and $\theta = \arctan B_y/B_z$ is the IMF clock-angle. This coupling function is dominated by IMF B_z, but it also includes IMF B_y. However, the Newell function (as all other coupling functions) is symmetric with respect to the sign of B_y.

Figures 3a and 3b show the average 30-80 keV proton fluxes in both hemispheres under positive ($> 20°$) dipole tilt. The proton fluxes are averaged over the dusk sector (12-24 MLT) and $\pm(55°...75°)$ corrected geomagnetic latitude, roughly corresponding to $L = 3-10$, which are the MLT and L-ranges with highest fluxes of protons in the CIMI results in Figure 1. The proton fluxes are binned by the Newell coupling function $d\Phi_{MP}/dt$ and IMF B_y averaged over 3 hours prior the proton measurements.

Figures 3a and 3b show that for a fixed value of $d\Phi_{MP}/dt$, the proton flux is clearly greater for $B_y < 0$ than for $B_y > 0$ in both hemispheres, in agreement with the above simulation results. The proton fluxes are generally higher in SH than NH, probably due to hemispheric asymmetry of magnetic field strength related to the South Atlantic Anomaly. Figures 3c and 3d further quantify the size of the B_y-dependence showing averages of the proton fluxes for $B_y < 0$ and $B_y > 0$ as a function of $d\Phi_{MP}/dt$. The standard errors in Figures 3c and 3d are calculated by normalizing the standard deviation on each bin by the square root of the number of samples. The B_y-effect is present in both hemispheres, although it is stronger for SH. Note that the flux units are shown in logarithmic scale.

Assuming that the fluxes measured by NOAA POES satellites (on low-Earth orbit) reflect patterns in underlying equatorial population, this result strongly supports the above CIMI results on B_y dependence of equatorial ring current fluxes.

Figure S2 in the supporting material shows the same analysis as Figure 3 for NH winter (dipole tilt $< -20°$). Figure S2 clearly shows that the B_y-dependence is reversed in the NH winter, in agreement with earlier studies on the explicit B_y-effect.

The above SWMF/CIMI model results also suggest that the Dst index exhibits an explicit B_y-dependence. To verify this, we make a similar analysis using the measured Dst, Dst^* index and their rate of change. Figure 4a shows the average measured Dst index as a function of 3-hour means of $d\Phi_{MP}/dt$ and IMF B_y during NH summer (dipole tilt $> 20°$) in the same format as in Figure 3. Figure 4a shows asymmetric pattern with respect to B_y, but the dependence it not so clear as for the proton precipitation. This is likely due the long memory of the Dst index, that is, there is a large lag between solar wind driving (coupling functions) and the response of the Dst index, because the value of Dst index for any give hour is mainly determined by the pre-existing ring current population. However, the time-derivative of the Dst index is known to have a more immediate response [*Burton et al.*, 1975; *Newell et al.*, 2007]. Indeed, there is a clear B_y-dependence in ΔDst (Figure 4b), which is the change of the Dst index over three hours. The B_y-dependence of Dst and ΔDst are further quantified in Figures 4c and 4d, which show the averages of the Dst index and ΔDst for $B_y < 0$ and $B_y > 0$ during different values of $d\Phi_{MP}/dt$. Analysis of error bars indicates that the effect is stronger for ΔDst and more statistically significant, but it is still present for Dst index as well.

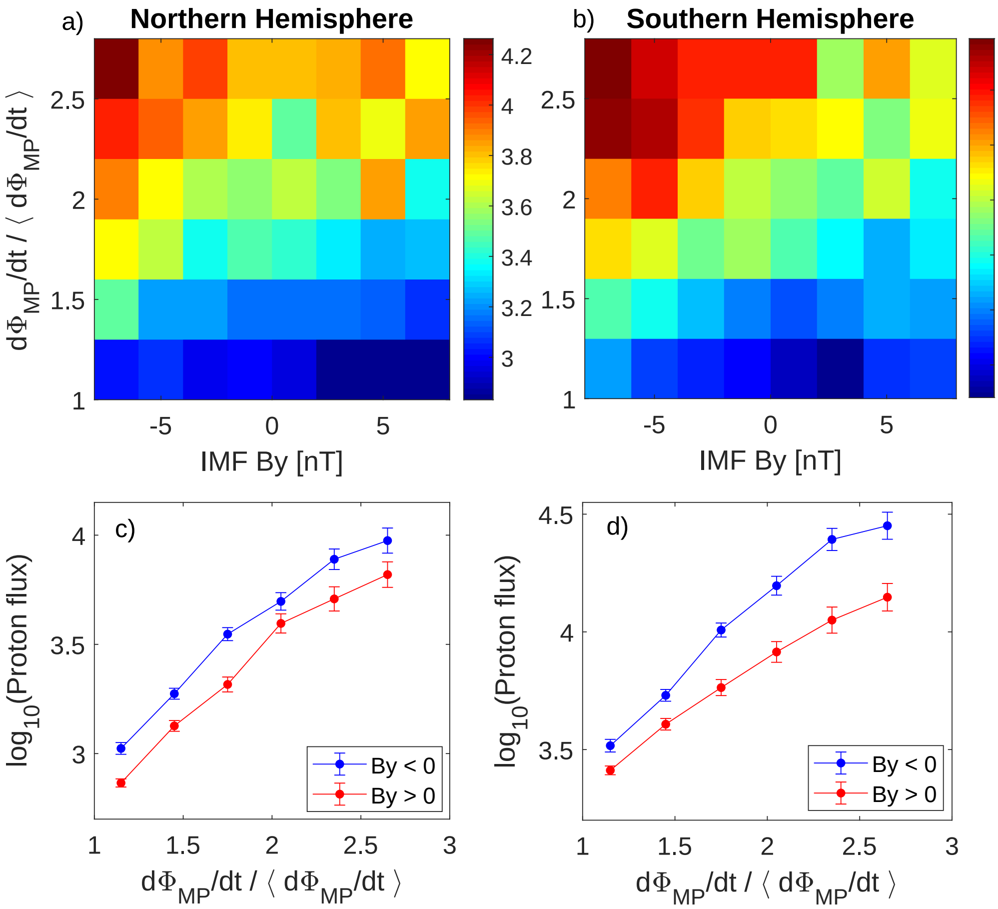

Figure 3. Flux of 30-80 keV protons measured by NOAA POES satellites as a function of 3-hour means of the Newell coupling function $d\Phi_{MP}/dt$ and IMF B_y during NH summer conditions (dipole tilt $> \ 20°$) a) in Northern Hemisphere ($55°...70°$ corrected geomagnetic latitude) b) Southern Hemisphere ($-55°... \ - \ 75°$ corrected geomagnetic latitude). The units are $1/\mathrm{cm}^2/\mathrm{sr/s}$ in log-10 scale. The Newell coupling function is normalized by its mean value in 1995-2019 $\langle d\Phi_{MP}/dt\rangle \ = \ 3.781 \cdot 10^3 \ (\mathrm{km/s})^{4/3}\mathrm{nT}^2/3$. c-d) Proton fluxes a-b) in averaged for $B_y \ < \ 0$ and $B_y \ < \ 0$ as a function of $d\Phi_{MP}/dt$. The vertical bars denote the standard errors of the means. Note the log scale for the proton flux.

Thus, the ring current grows at a faster rate ($-\Delta Dst$ is greater) for $B_y < 0$ during positive dipole tilt, confirming the CIMI modeling results on the ring current energy content and model Dst index (Fig. 2). Figures S3a and S3b show the same analysis of Dst and ΔDst for negative ($< -20°$) dipole tilt. The B_y-dependence during negative tilt is reversed (faster growth of the ring current for $B_y > 0$) which is also expected from earlier studies on the explicit B_y-effects. The B_y-dependence in the time-derivative of the Dst-index is quite strong. For the highest values of the Newell coupling function shown in Figure 4d ΔDst is about 50% greater for $B_y < 0$ than for $B_y > 0$. In order to have sufficient statistics, data in Figure 4 are limited to mainly non-storm times (as seen in the scale of Dst values in Figure 4a). Further modeling and event studies are needed for studying how significant the B_y-dependence is during storm-times. Figures S3c-S3d and S3e-S3f repeat the analysis of Figure 4 for positive and negative dipole tilts using the pressure-corrected Dst index (Dst^*) [*O'Brien and McPherron*, 2000], yielding practically identical results. This gives confidence that the results of Figure 4 are not contaminated by the magnetopause current.

Taken together, the analysis of NOAA POES data and Dst index gives strong evidence that there is a *global* explicit IMF B_y-effect in magnetospheric energetic protons and ring current energy content. These findings are strongly supported by the above SWMF/CIMI results as well.

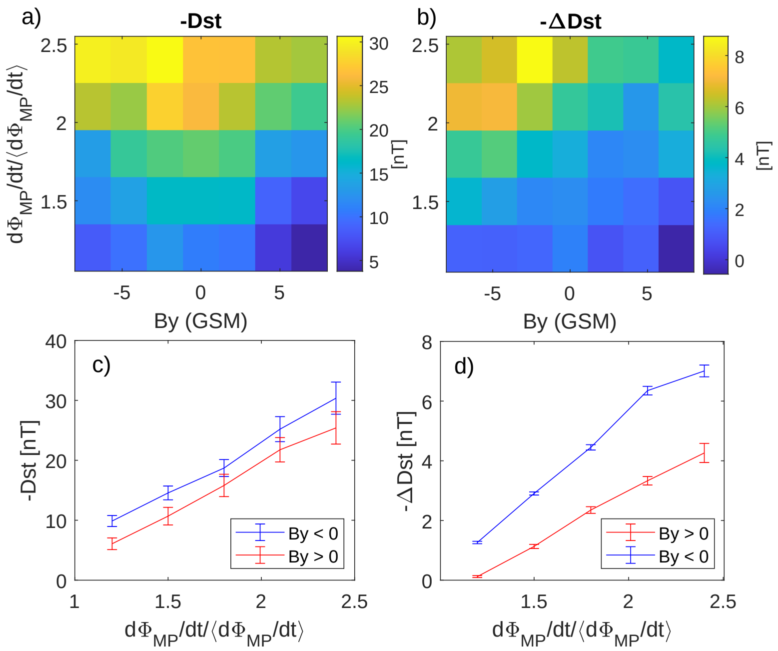

Figure 4. a) The Dst index as a function of 3-hour means of the Newell coupling function $d\Phi_{MP}/dt$ and IMF B_y in NH summer (dipole tilt $>$ 20°). b) The change of the Dst index (ΔDst) during the same three-hour intervals as in the panel a). Bottom panels show c) Dst d) ΔDst averaged for $B_y < 0$ (blue line) and $B_y > 0$ (red line) as a function of Φ_{MP}/dt. The vertical bars denote the standard errors of the means.

5 Discussion and Conclusions

It has been known for a long time that IMF B_y plays a role in solar wind-magnetosphere interaction which is seen, e.g., convection patterns in polar caps and auroral zones [*Heppner and Maynard*, 1987; *Cowley et al.*, 1991; *Ruohoniemi and Greenwald*, 1996, 2005; *Thomas and Shepherd*, 2018]. Recent studies have revealed that IMF B_y effects are complex and seasonally varying, showing dependence on the dipole tilt angle. The combined dependence on IMF B_y and the dipole tilt (also called the explicit B_y-dependence) strongly modulates auroral electrojets [*Friis-Christensen et al.*, 2017; *Holappa and Mursula*, 2018; *Holappa et al.*, 2021; *Workayehu et al.*, 2021], electron precipitation [*Holappa et al.*, 2020], and the size of polar cap [*Reistad et al.*, 2020]. These effects are quite significant, for example showing variations in the AL index up to 40% for opposite values of B_y.

In this paper, using a global MHD/ring current model and satellite measurements we have demonstrated, for the first time, a global explicit IMF B_y-dependence of the ring current proton fluxes, and the Dst index. We showed that IMF B_y-component significantly modulates energetic magnetospheric protons, the time-derivative of the Dst index and consequently the growth-rate of the ring current.

First we performed two simulations with the SWMF coupled with the CIMI inner magnetosphere model with static solar wind/IMF inputs ($V = 500$ km/s, $B_z = -5$ nT) and positive (+20°) dipole tilt. The two runs had identical solar wind inputs and other settings except for the sign of IMF B_y. We found that the run with negative B_y produced stronger fluxes of energetic protons in the inner magnetosphere.

To verify the model results we quantified the explicit B_y-dependence of the energetic (30−80 keV) magnetospheric proton fluxes measured by NOAA POES satellites flying on polar low-Earth orbits. We showed that for fixed value of the Newell solar wind coupling function ($d\Phi_{MP}/dt$) the NOAA POES proton fluxes are greater for $B_y < 0$ than for $B_y > 0$ in northern hemisphere summer (dipole tilt $> 20°$). These empirical results are in excellent agreement with the model results, assuming that the proton fluxes measured by NOAA POES satellites on low-Earth orbit reflect the modeled equatorial ring current protons with similar energy (IMF B_y not significantly modulating the pitch-angle distribution).

Because the ring current is mainly carried by energetic protons in the inner magnetosphere, the above results indicate that the ring current energy content and the Dst index should also exhibit an explicit IMF B_y dependence. Indeed, we found that the SWMF/CIMI run with a negative IMF B_y produced a greater energy content of the ring current and a more negative modeled Dst index. To verify this empirically, we showed that for a fixed value of $d\Phi_{MP}/dt$ the measured Dst index, Dst^* index and the time-derivative of Dst and Dst^* $(\Delta Dst, \Delta Dst^*)$ is more negative for $B_y < 0$ during positive dipole tilt.

Thus, for fixed solar wind driving the ring current grows faster and becomes stronger for $B_y < 0$ ($B_y > 0$) in northern hemisphere summer (winter). Therefore the ring current growth-rate exhibits a similar explicit B_y-dependence as the westward electrojet [*Holappa and Mursula*, 2018] and substorm occurrence frequency [*Ohma et al.*, 2021].

The physical mechanism(s) of the explicit B_y-effects on the magnetospheric dynamics and particularly on the inner magnetosphere are still not fully understood. Recently, *Reistad et al.* [2020] showed that the polar cap area exhibits a similar explicit B_y-dependence: during positive tilt polar cap is larger for $B_y < 0$ than for $B_y > 0$ while the B_y-dependence is opposite for negative dipole tilt. They suggested that IMF B_y either modulates the dayside reconnection rate or the magnetotail response to solar wind driving. Evidence toward the former hypothesis was provided by *Reistad et al.* [2021] who showed that there is an explicit B_y-dependence in the cross-polar cap potential which is consistent with a similar B_y-dependence of the substorm occurrence frequency [*Ohma et al.*, 2021].

The IMF B_y-dependence of the energetic proton fluxes and the ring current in the inner magnetosphere is probably closely related to the B_y-dependence of substorm activity, as substorms are known to cause injections of energetic particles into the inner magnetosphere [*Mauk and McIlwain*, 1974; *Birn et al.*, 1998; *Gkioulidou et al.*, 2014]. Another explanation is suggested by results from ring current models showing that electric field in the inner magnetosphere controls the strength of the ring current (e.g., *Ebihara and Ejiri* [2003]). In order to get stronger ring current in the coupled model, there should be stronger potential drop and stronger convection near the ring current model polar boundary, that is, on closed magnetic field lines. From this perspective it would be interesting to reanalyze the results of *C:son Brandt et al.* [2002] to examine if strong IMF B_y produces additional skewing of the electric field in the inner magnetosphere. Multiple studies confirm that the presence of IMF B_y is not needed for the skewing since it is produced by the ring current itself [*Wolf*, 1983; *Fok et al.*, 2003; *Ebihara and Fok*, 2004; *Buzulukova et al.*, 2010b]. However, the results of our study suggest that indeed some additional effect is possible since the strength of the ring current is modulated by IMF B_y. At present, it is not clear why the convection on the closed field lines should be stronger when the signs of IMF B_y and dipole tilt are opposite. However the reproduction of the effect with the coupled SWMF/CIMI model demonstrates the potential of future modeling studies to uncover the physical mechanism of the explicit B_y-effect. Further modeling and event-based studies are also also needed for studying how significant the explicit B_y-dependence of the ring current is during storm-times.

Acknowledgments

We acknowledge the financial support by the Academy of Finland to the Postdoctoral Researcher project of LH (no. 322459). For N. B., this work has been partially supported by NASA grant 80NSSC19K0085. N.B. thanks ISSI in Bern Switzerland for support of the International Team N523 "Imaging the Invisible: Unveiling the Global Structure of Earth's Dynamic Magnetosphere". This work was carried out using the SWMF and BATS-R-US tools developed at the University of Michigan's Center for Space Environment Modeling (CSEM). The modeling tools are available through the University of Michigan for download under a user license. The open source version of SWMF could be downloaded from https://github.com/MSTEM-QUDA. CIMI model has been developed at NASA GSFC, Heliophysics division, Geospace Physics Laboratory. Computational resources supporting this work were provided by the NASA High-End Computing (HEC) Program through the NASA Advanced Supercomputing (NAS) Division at Ames Research Center.

6 Data availability statement

The solar wind data (solar wind speed and different components of IMF) were downloaded from the OMNI2 database (`http://omniweb.gsfc.nasa.gov/`). All the original POES/MEPED energetic particle data used here are archived in the NOAA/NGDC dataserver (`http://www.ngdc.noaa.gov/stp/satellite/poes/index.html`). The University of Oulu *Dst* index was downloaded from `https://dcx.oulu.fi`. Model output used in production of Figures 1 and 2 have been made available online for download at Zenodo `https://zenodo.org/record/5893998.Yez5jVmxVEY`, DOI:10.5281/zenodo.5893998.

References

Asikainen, T., and K. Mursula (2011), Recalibration of the long-term NOAA/MEPED energetic proton measurements, *J. Atm. Sol.-Terr. Phys.*, *73*(2-3), 335–347.

Asikainen, T., and K. Mursula (2013), Correcting the NOAA/MEPED energetic electron fluxes for detector efficiency and proton contamination, *J. Geophys. Res.*, *118*(10), 6500–6510.

Birn, J., and M. Hesse (2013), The substorm current wedge in mhd simulations, *Journal of Geophysical Research: Space Physics*, *118*(6), 3364–3376, doi: https://doi.org/10.1002/jgra.50187.

Birn, J., M. F. Thomsen, J. E. Borovsky, G. D. Reeves, D. J. McComas, R. D. Belian, and M. Hesse (1998), Substorm electron injections: Geosynchronous observations and test particle simulations, , *103*(A5), 9235–9248, doi:10.1029/97JA02635.

Burton, R. K., R. L. McPherron, and C. T. Russell (1975), An empirical relationship between interplanetary conditions and dst, *J. Geophys. Res.*, *80*(31), 4204–4214.

Buzulukova, N., M.-C. Fok, A. Pulkkinen, M. Kuznetsova, T. E. Moore, A. Glocer, P. C. Brandt, G. Toth, and L. Rastätter (2010a), Dynamics of ring current and electric fields in the inner magnetosphere during disturbed periods: CRCM–BATS-R-US coupled model, *J. Geophys. Res. Space Physics*, *115*(A5).

Buzulukova, N., M.-C. Fok, J. Goldstein, P. Valek, D. J. McComas, and P. C. Brandt (2010b), Ring current dynamics in moderate and strong storms: Comparative analysis of twins and image/hena data with the comprehensive ring current model, *Journal of Geophysical Research: Space Physics*, *115*(A12), doi: https://doi.org/10.1029/2010JA015292.

Cowley, S. W. H., J. P. Morelli, and M. Lockwood (1991), Dependence of convective flows and particle precipitation in the high-latitude dayside ionosphere on the x and y components of the interplanetary magnetic field, *J. Geophys. Res.*, *96*(A4), 5557–5564.

C:son Brandt, P., S. Ohtani, D. G. Mitchell, M.-C. Fok, E. C. Roelof, and R. Demajistre (2002), Global ena observations of the storm mainphase ring current: Implications for skewed electric fields in the inner magnetosphere, *Geophysical Research Letters*, *29*(20), 15–1–15–3, doi:https://doi.org/10.1029/2002GL015160.

de Zeeuw, D. L., S. Sazykin, R. A. Wolf, T. I. Gombosi, A. J. Ridley, and G. Tóth (2004), Coupling of a global MHD code and an inner magnetospheric model: Initial results, *Journal of Geophysical Research (Space Physics)*, *109*(A12), A12219, doi:10.1029/2003JA010366.

Dessler, A. J., and E. N. Parker (1959), Hydromagnetic theory of geomagnetic storms, *J. Geophys. Res.*, *64*(12), 2239–2252.

Dungey, J. W. (1961), Interplanetary magnetic field and the auroral zones, *Phys. Rev. Lett*, *6*, 47–49.

Ebihara, Y., and M. Ejiri (2003), Numerical Simulation of the Ring Current: Review, , *105*(1), 377–452, doi:10.1023/A:1023905607888.

Ebihara, Y., and M. C. Fok (2004), Postmidnight storm-time enhancement of tens-of-keV proton flux, *Journal of Geophysical Research (Space Physics)*, *109*(A12), A12209, doi:10.1029/2004JA010523.

Fedder, J. A., S. P. Slinker, J. G. Lyon, and R. D. Elphinstone (1995), Global numerical simulation of the growth phase and the expansion onset for a substorm observed by viking, *Journal of Geophysical Research: Space Physics*, *100*(A10), 19,083–19,093, doi:https://doi.org/10.1029/95JA01524.

Fok, M. C., T. E. Moore, G. R. Wilson, J. D. Perez, X. X. Zhang, P. C. S. Brandt, D. G. Mitchell, E. C. Roelof, J. M. Jahn, C. J. Pollock, and R. A. Wolf (2003), Global ena Image Simulations, , *109*(1), 77–103, doi:10.1023/B:SPAC.0000007514.56380.fd.

Fok, M.-C., N. Y. Buzulukova, S.-H. Chen, A. Glocer, T. Nagai, P. Valek, and J. D. Perez (2014), The comprehensive inner magnetosphere-ionosphere model, *J. Geophys. Res. Space Physics*, *119*(9), 7522–7540.

Fok, M.-C., S.-B. Kang, C. P. Ferradas, N. Y. Buzulukova, A. Glocer, and C. M. Komar (2021), New Developments in the Comprehensive Inner Magnetosphere-Ionosphere Model, *J. Geophys. Res. Space Physics*, *126*(4), e2020JA028,987.

Friis-Christensen, E., K. Lassen, J. Wilhjelm, J. M. Wilcox, W. Gonzalez, and D. S. Colburn (1972), Critical component of the interplanetary magnetic field responsible for large geomagnetic effects in the polar cap, *J. Geophys. Res.*, *77*(19), 3371–3376, doi:10.1029/JA077i019p03371.

Friis-Christensen, E., C. C. Finlay, M. Hesse, and K. M. Laundal (2017), Magnetic Field Perturbations from Currents in the Dark Polar Regions During Quiet Geomagnetic Conditions, *Space Sci. Rev.*, *206*(1-4), 281–297.

Gkioulidou, M., A. Y. Ukhorskiy, D. G. Mitchell, T. Sotirelis, B. H. Mauk, and L. J. Lanzerotti (2014), The role of small-scale ion injections in the buildup of Earth's ring current pressure: Van Allen Probes observations of the 17 March 2013 storm, *J. Geophys. Res. Space Physics*, *119*(9), 7327–7342.

Glocer, A., M. Fok, X. Meng, G. Toth, N. Buzulukova, S. Chen, and K. Lin (2013), CRCM+ BATS–R–US two–way coupling, *J. Geophys. Res. Space Physics*, *118*(4), 1635–1650.

Gordeev, E., V. Sergeev, N. Tsyganenko, M. Kuznetsova, L. Rastäetter, J. Raeder, G. Tóth, J. Lyon, V. Merkin, and M. Wiltberger (2017), The substorm cycle as reproduced by global mhd models, *Space Weather*, *15*(1), 131–149, doi: https://doi.org/10.1002/2016SW001495.

Hamilton, D. C., G. Gloeckler, F. Ipavich, W. Stüdemann, B. Wilken, and G. Kremser (1988), Ring current development during the great geomagnetic storm of february 1986, *J. Geophys. Res.*, *93*(A12), 14,343–14,355.

Heppner, J. P., and N. C. Maynard (1987), Empirical high-latitude electric field models, *J. Geophys. Res.*, *92*(A5), 4467–4489.

Holappa, L., and K. Mursula (2018), Explicit IMF B_y-dependence in high-latitude geomagnetic activity, *J. Geophys. Res.*, *123*, 4728–4740, doi: 10.1029/2018JA025517.

Holappa, L., T. Asikainen, and K. Mursula (2020), Explicit IMF Dependence in Geomagnetic Activity: Modulation of Precipitating Electrons, *Geophys. Res. Lett.*, *47*(4), e2019GL086,676.

Holappa, L., R. M. Robinson, A. Pulkkinen, T. Asikainen, and K. Mursula (2021), Explicit IMF By-Dependence in Geomagnetic Activity: Quantifying Ionospheric Electrodynamics, *J. Geophys. Res. Space Physics*, *126*(4), e2021JA029,202.

Karinen, A., and K. Mursula (2005), A new reconstruction of the Dst index for 1932-2002, *Ann. Geophys.*, *23*, 475–485.

Keesee, A. M., N. Buzulukova, C. Mouikis, and E. E. Scime (2021), Mesoscale structures in earth's magnetotail observed using energetic neutral atom imaging, *Geophysical Research Letters*, *48*(3), e2020GL091,467, doi: https://doi.org/10.1029/2020GL091467, e2020GL091467 2020GL091467.

Laitinen, T. V., M. Palmroth, T. I. Pulkkinen, P. Janhunen, and H. E. J. Koskinen (2007), Continuous reconnection line and pressure-dependent energy conversion on the magnetopause in a global mhd model, *J. Geophys. Res.*, *112*(A11).

Liemohn, M. W., J. U. Kozyra, M. F. Thomsen, J. L. Roeder, G. Lu, J. E. Borovsky, and T. E. Cayton (2001), Dominant role of the asymmetric ring current in producing the stormtime dst, *J. Geophys. Res. Space Physics*, *106*(A6), 10,883–10,904.

Mauk, B. H., and C. E. McIlwain (1974), Correlation of Kp with the substorm-injected plasma boundary, , *79*(22), 3193–3196, doi:10.1029/JA079i022p03193.

Merkin, V. G., E. V. Panov, K. A. Sorathia, and A. Y. Ukhorskiy (2019), Contribution of bursty bulk flows to the global dipolarization of the magnetotail during an isolated substorm, *Journal of Geophysical Research: Space Physics*, *124*(11), 8647–8668, doi:https://doi.org/10.1029/2019JA026872.

Mursula, K., L. Holappa, and A. Karinen (2008), Correct normalization of the Dst index, *Astrophys. Space Sci. Transact.*, *4*, 41–45, doi:10.5194/astra-4-41-2008.

Newell, P. T., T. Sotirelis, K. Liou, C.-I. Meng, and F. J. Rich (2007), A nearly universal solar wind-magnetosphere coupling function inferred from 10 magnetospheric state variables, *J. Geophys. Res.*, *112*(A1).

O'Brien, T. P., and R. L. McPherron (2000), An empirical phase space analysis of ring current dynamics: Solar wind control of injection and decay, *J. Geophys. Res. Space Physics*, *105*(A4), 7707–7719.

Ohma, A., J. P. Reistad, and S. M. Hatch (2021), Modulation of Magnetospheric Substorm Frequency: Dipole Tilt and IMF By Effects, *J. Geophys. Res. Space Physics*, *126*(3), e2020JA028,856.

Raeder, J., P. Zhu, Y. Ge, and G. Siscoe (2010), Open geospace general circulation model simulation of a substorm: Axial tail instability and ballooning mode preceding substorm onset, *Journal of Geophysical Research: Space Physics*, *115*(A5), doi:https://doi.org/10.1029/2010JA015876.

Reistad, J. P., K. M. Laundal, A. Ohma, T. Moretto, and S. E. Milan (2020), An Explicit IMF By Dependence on Solar Wind-Magnetosphere Coupling, *Geophys. Res. Lett.*, *47*(1), e2019GL086,062.

Reistad, J. P., K. M. Laundal, N. Østgaard, A. Ohma, A. G. Burrell, S. M. Hatch, S. Haaland, and E. G. Thomas (2021), Quantifying the lobe reconnection rate during dominant imf by periods and different dipole tilt orientations, *J. Geophys. Res. Space Physics*, p. e2021JA029742.

Ridley, A. J., T. I. Gombosi, and D. L. DeZeeuw (2004), Ionospheric control of the magnetosphere: conductance, *Annales Geophysicae*, *22*(2), 567–584, doi: 10.5194/angeo-22-567-2004.

Ruohoniemi, J. M., and R. A. Greenwald (1996), Statistical patterns of high-latitude convection obtained from Goose Bay HF radar observations, *J. Geophys. Res.*, *101*(A10), 21,743–21,763, doi:10.1029/96JA01584.

Ruohoniemi, J. M., and R. A. Greenwald (2005), Dependencies of high-latitude plasma convection: Consideration of interplanetary magnetic field, seasonal, and universal time factors in statistical patterns, *J. Geophys. Res.*, *110*(A9).

Smith, A. R. A., C. D. Beggan, S. Macmillan, and K. A. Whaler (2017), Climatology of the auroral electrojets derived from the along-track gradient of magnetic field intensity measured by POGO, Magsat, CHAMP, and Swarm, *Space Weather*, *15*(10), 1257–1269, doi:10.1002/2017SW001675, 2017SW001675.

Sonnerup, B. U. O. (1974), Magnetopause reconnection rate, *J. Geophys. Res.*, *79*(10), 1546–1549, doi:10.1029/JA079i010p01546.

Thomas, E. G., and S. G. Shepherd (2018), Statistical patterns of ionospheric convection derived from mid-latitude, high-latitude, and polar SuperDARN HF radar observations, *J. Geophys. Res.*, *123*(4), 3196–3216.

Tóth, G., I. V. Sokolov, T. I. Gombosi, D. R. Chesney, C. R. Clauer, D. L. De Zeeuw, K. C. Hansen, K. J. Kane, W. B. Manchester, R. C. Oehmke, et al. (2005), Space Weather Modeling Framework: A new tool for the space science community, *J. Geophys. Res.*, *110*(A12).

Trattner, K. J., S. M. Petrinec, S. A. Fuselier, and T. D. Phan (2012), The location of reconnection at the magnetopause: Testing the maximum magnetic shear model with themis observations, *J. Geophys. Res. Space Physics*, *117*(A1).

Weimer, D., and T. Edwards (2021), Testing the electrodynamic method to derive height-integrated ionospheric conductances, *Ann. Geophys.*, *39*(1), 31–51.

Wolf, R. A. (1983), The quasi-static (slow-flow) region of the magnetosphere, in *Solar-Terrestrial Physics: Principles and Theoretical Foundations*, *Astrophysics and Space Science Library*, vol. 104, edited by R. L. Carovillano and J. M. Forbes, pp. 303–368, doi:10.1007/978-94-009-7194-3_14.

Workayehu, A. B., H. Vanhamäki, A. T. Aikio, and S. G. Shepherd (2021), Effect of Interplanetary Magnetic Field on Hemispheric Asymmetry in Ionospheric Horizontal and Field-Aligned Currents During Different Seasons, *J. Geophys. Res. Space Physics*, *126*(10), e2021JA029,475.

Yakovchouk, O. S., K. Mursula, L. Holappa, I. S. Veselovsky, and A. Karinen (2012), Average properties of geomagnetic storms in 1932-2009, *J. Geophys. Res.*, *117*, A03201, doi:10.1029/2011JA017093.

Zhang, M. W., J.and Liemohn, D. L. De Zeeuw, J. E. Borovsky, A. J. Ridley, G. Toth, S. Sazykin, M. F. Thomsen, J. U. Kozyra, and T. I. Gombosi (2007), Understanding storm-time ring current development through data-model comparisons of a moderate storm, *J. Geophys. Res. Space Physics*, *112*(A4).

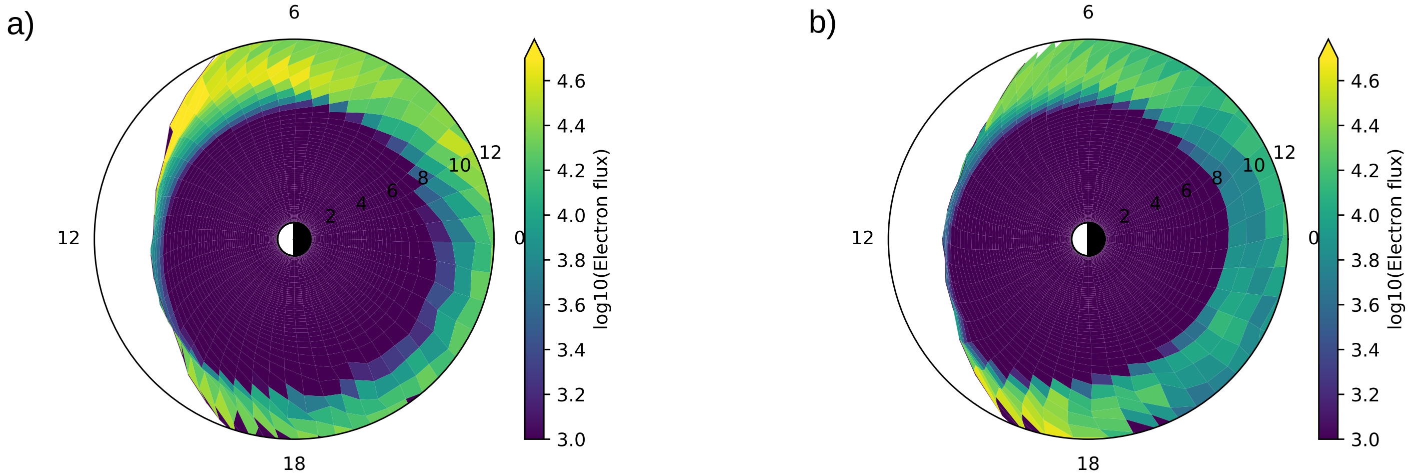

Figure S1. Equatorial omnidirectional fluxes of 56 keV electrons for a) the run with By<0 b) By>0. The fluxes are shown for the last timesteps (8.00 h) of the two runs. Sun is from the left. Labels indicate magnetic local time and radial distance (in Earth radii).

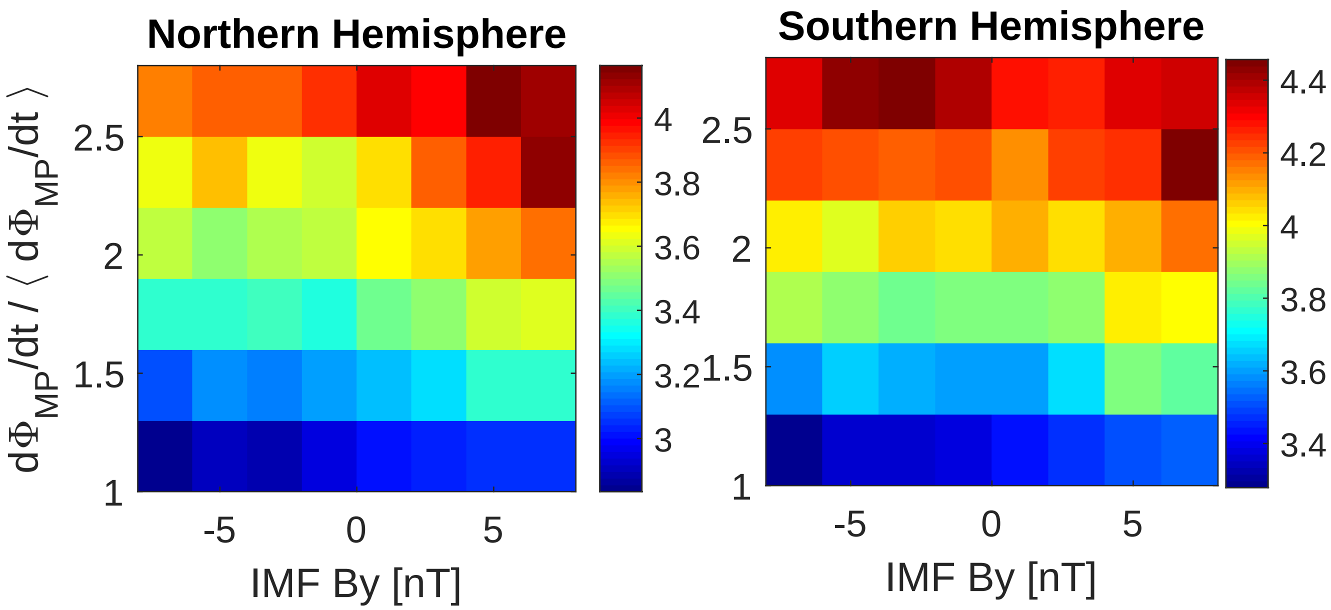

Figure S2. Flux of 30-80 keV protons measured by NOAA POES satellites as a function of 3-hour means of the Newell coupling function and IMF By during NH winter conditions (dipole tilt < -20 degrees) a) in Northern Hemisphere (55...75 degrees corrected geomagnetic latitude) b) Southern Hemisphere (55...-75 degrees corrected geomagnetic latitude).

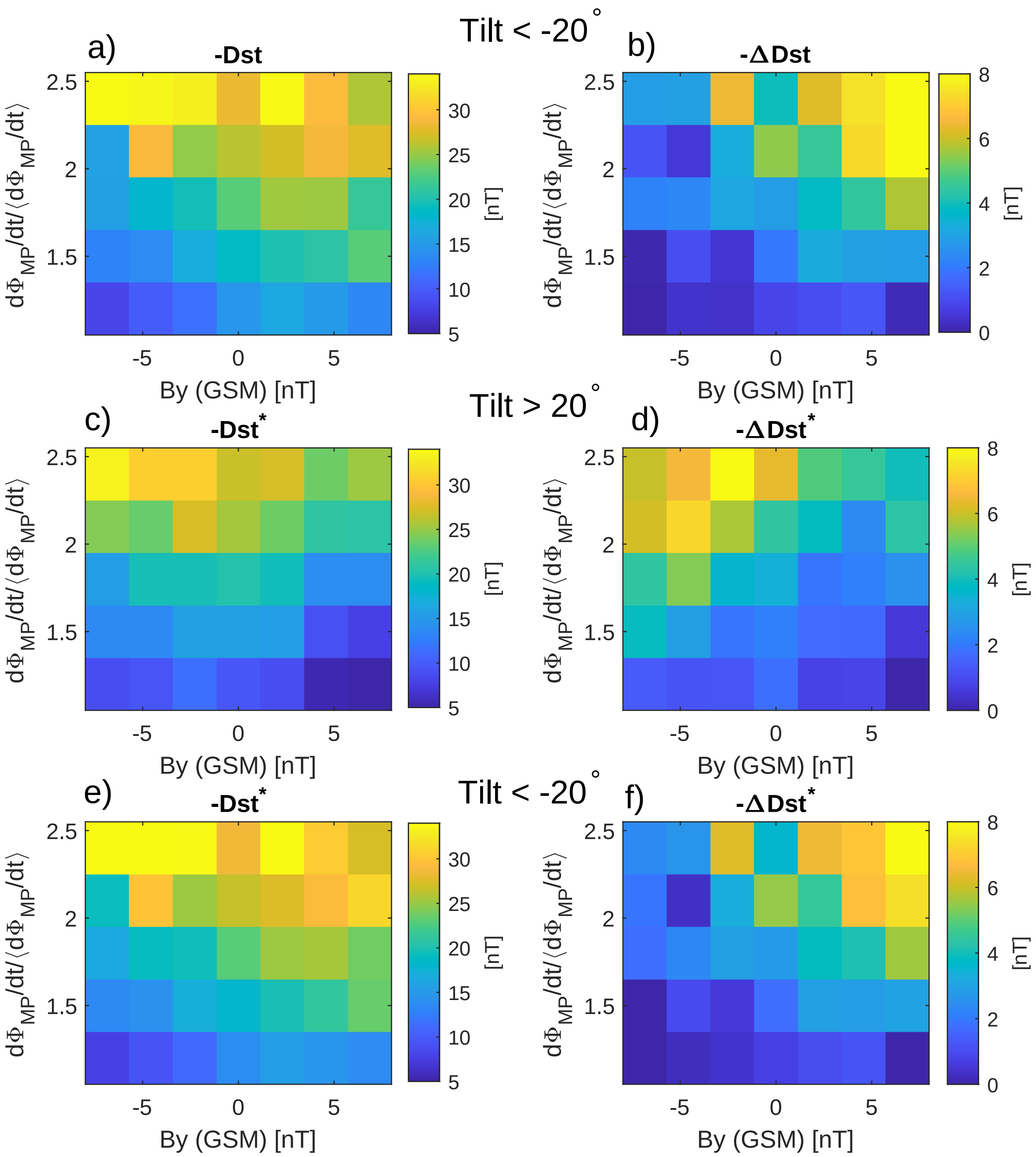

Figure S3. a) The Dst index as a function of 3-hour means of the Newell coupling function and IMF By in NH winter (dipole tilt <-20 degrees). b) The change of the Dst index during the same three-hour intervals as in the panel a). Panels c-d) are similar to panels a-b) but are calculated for positive (>20 degrees) dipole tilt and for the pressure-corrected Dst index (Dst*). Panels e-f) are similar to panels c-d) but are calculated for negative dipole tilt (<-20 degrees).